Low vapor pressure solvents for single-molecule junction measurements

Leopold Kim,† Thomas M. Czyszczon-Burton,† Kenneth M. Nguyen, Samantha Stukey, Sawyer Lazar, Jazmine Prana, Zelin Miao, Seongje Park, Sully F. Chen, and Michael S. Inkpen*

Department of Chemistry, University of Southern California, Los Angeles, CA 90089, USA

E-mail: inkpen@usc.edu

† L.K. and T.M.C.B. contributed equally to this work.

ABSTRACT

Non-polar solvents commonly used in scanning tunneling microscope-based break junction measurements exhibit hazards and relatively low boiling points (b.p.) that limit the scope of solution experiments at elevated temperatures. Here we show that low toxicity, ultra-high b.p. solvents such as bis(2-ethylhexyl) adipate (b.p. = 417°C) and squalane (457°C) can be used to probe molecular junctions at ≥100°C. With these, we extend solvent- and temperature-dependent conductance trends for junction components such as 4,4'-bipyridine and thiomethyl-terminated oligophenylenes and reveal the gold snapback distance is larger at 100°C due to increased surface atom mobility. We further show the rate of surface transmetallation and homocoupling reactions using phenylboronic acids increases at 100°C, while junctions comprising anticipated boroxine condensation products form only at room temperature in an anhydrous glovebox atmosphere. Overall, this work demonstrates the utility of low vapor pressure solvents for the comprehensive characterization of junction properties and chemical reactivity at the single-molecule limit.

KEY WORDS

single-molecule junctions, non-polar solvents, in situ reactions, boronic acids, temperature-dependent conductance

Non-polar solvents such as 1,2,4-trichlorobenzene (TCB) or 1-phenyloctane (PO) are widely used in scanning tunneling microscope (STM) experiments for surface self-assembly[1,2] or single-molecule conductance[3–5] studies. The moderately high boiling points (b.p.) of these and other commonly-used non-conducting compounds (b.p. = 165-271°C, **Table 1**) mitigate their evaporation at room temperature (RT) and minimize Faradaic and capacitive currents that complicate measurements in media of higher polarity.[6] While the solvent environment is key to achieving sufficient analyte dissolution, is can also control interfacial charge transport and chemical reactivity. In STM-based break junction (STM-BJ) experiments, solvents comprising heteroatoms with a relatively high binding affinity for gold have been found to influence the energetic level alignment between the dominant conducting orbital(s) of the molecule and the Fermi level (E_F) of the electrodes, rendering junction tunneling conductance solvent-dependent.[7–10] One such solvent, 1-bromonapthalene (BN), can even influence the most probable binding geometry of gold-thiol junctions by effectively competing for undercoordinated surface sites.[11] Should charge hopping processes dominate transport, the solvent environment around the junction may also impact conductance by modulating the outer sphere reorganization energies associated with sequential electron transfer events.[12–14] The solvent dielectric can also tune the strength of interfacial electric fields shown to catalyze *in situ* chemical transformations.[15,16]

Critically, most non-polar solvents do not exhibit sufficiently low vapor pressures to inhibit significant evaporation at elevated temperatures or over extended periods at RT.[9] To minimize the impact of varying solution concentration, previous studies have measured samples at high temperatures prior to low temperature[5] or have periodically added pure solvent to analyte solutions.[16] We propose that new, robust strategies to minimize solvent loss could enable several useful studies and comparison experiments, including: (1) precise control of reagent concentrations to probe the kinetics of *in situ* chemical reactions; (2) use of high temperatures to drive *in situ* chemical reactions that are unfavorable at RT; (3) rigorous assessment of thermally-triggered molecular switches;[17] or (4) the evaluation of single-molecule charge transport mechanisms (tunneling vs. hopping).[7,18] It has been suggested that more studies of molecular junctions at >85°C, the likely operating temperature of hybrid molecule-semiconductor integrated circuits, are needed to fully evaluate their potential technological applications.[19] We also note that the volatilization of hazardous solvents such as TCB through extended use or deliberate heating is a potential health hazard. This may prove particularly problematic in typical low airflow laboratory environments housing STM instrumentation, where acoustic isolation/electromagnetic shielding chambers concentrate

solvent vapors. There is a clear need to identify ultra-high b.p., low toxicity solvents for STM studies, particularly for experiments at elevated temperatures.

In this work, we introduce bis(2-ethylhexyl) adipate (DEHA) and squalane (SQ) as safe, low vapor pressure solvents that facilitate STM experiments at temperatures ≥100°C over extended periods (≥1 d). As part of a wider solvent survey, we first demonstrate that both N lone pair and pyridyl π-coordinated 4,4'-bipyridine (**bipy**) junctions successfully form from DEHA and SQ solutions at RT.[20] We subsequently show that junctions formed from thioether-terminated oligophenyls in DEHA at 100°C exhibit not only an increased conductance compared to RT, corroborating a recent report,[5] but also a decreased junction step length. Snapback measurements indicate that the change in step length is due to the increased mobility of gold at elevated temperatures that results in faster electrode restructuring after breaking atomic point contacts. Finally, studies of phenylboronic acids in DEHA show that the rate of previously reported *in situ* $C(sp^2)$-$C(sp^2)$ bond forming reactions[21] is significantly increased at 100°C relative to RT. Despite driving off water in studies at ≥100°C we find no evidence for boronic acid condensation reactions in air, in stark contrast to glovebox STM-BJ measurements performed at RT in an anhydrous nitrogen atmosphere which are dominated by the boroxine cyclotrimerization product. Taken together, we anticipate the methods and findings introduced in this study will prove critical for evaluating the potential impact of time and elevated temperature on the conductance, stability, and function of molecular-scale junctions formed from solution.

In **Table 1** we first consolidate key metrics for established and new non-polar STM-BJ solvents (for chemical structures, see **Figure 1a** and **SI, Figure S2**). Entries 1-5 comprise solvents commonly utilized for STM-BJ studies that may reasonably be considered to exhibit high b.p.: TCB,[3–5] 1,3,5-trimethylbenzene (mes),[22] tetradecane (TD),[23] BN,[7,12] and PO.[5] However, we find that the small quantities of TCB typically used in STM experiments (25 mg) completely evaporate at 100°C after 1 h (**SI, Solvent Evaporation Studies**). This rapid loss of solvent imposes experimental limitations as indicated in a recent study of the temperature-dependent conductance of oligophenylene wires, in which the maximum temperature reported for measurements in TCB was 55°C (in PO, 73°C).[5] Notably, all of these commonly used solvents exhibit specific hazards as reported in the Material Safety Data Sheets obtained from commercial suppliers (red rows, **Table 1**).

Table 1. Selected properties of non-polar STM-BJ solvents explored in this work.[a]

#	solvent	m.p. (°C)	b.p. (°C)	LD50 (mg/kg)[b]	hazards[c]
1	1,2,4-trichlorobenzene (TCB)	17	214	930	H, A
2	1,3,5-trimethylbenzene (mes)	−45	165	6,000	H, A
3	tetradecane (TD)	5.5	~253	>5,000	H
4	1-bromonapthalene (BN)	~−2	~271	810	H
5	phenyloctane (PO)	−36	~262	-[d]	-[d]
6	dibutyl maleate (mal)	−85	280	≥3,730	H
7	hexadecane (HD)	18	287	>5,000	H
8	1-octadecene (OD)	~16	315	>2,000	H
9	bis(2-ethylhexyl) adipate (DEHA)	−68	417	>20,000	-
10	squalane (SQ)	−38	457	-	-

[a] Chemical structures shown in **Figure 1** and **SI, Figure S2**. Table rows are shaded to indicate key solvent characteristics: red = commonly used, hazardous; orange = infrequently used, hazardous, higher boiling point (b.p.); underutilized, non-toxic, ultra-high b.p. [b] From Material Safety Data Sheets, the amount of an orally administered material which causes the death of 50% of a population of rats, and [c] notable hazards include H = hazardous (*skin irritant/sensitizer*, *toxic to organs*, or *may be fatal if swallowed*) or A = *toxic to aquatic life*. [d] Hazards not fully characterized.

We sought to identify other compounds with melting points <25°C and b.p. >271°C. While dibutyl maleate (mal), hexadecane (HD), and 1-octadecene (OD) qualify, they still pose significant hazards (orange rows, **Table 1**). In contrast, DEHA and SQ fall into a distinct category, having both ultra-high b.p. (≥417°C) and low toxicity (green rows, **Table 1**). While the environmental health impact of DEHA is still under active evaluation, it is a commonly used plasticizer in food packaging with >14,500 tons produced annually in the US and EU, combined.[24] A branched alkane with formula $C_{30}H_{62}$, SQ is a naturally occurring component of human sebum and a widely used cosmetic ingredient.[25] Remarkably, we find that small quantities (29-84 mg) of DEHA or SQ can be heated to 100°C for 1 d with <4% mass loss. This indicates these solvents could be used to perform STM studies at ≥100°C, a milestone temperature for exploring chemical dynamics and reactivity under ambient pressure. Such experiments approach the limit of variable-temperature nuclear magnetic resonance spectroscopy (facilitating useful comparison studies) and have the potential to drive *in situ* condensation reactions by generating an anhydrous environment that shifts the position of associated chemical equilibria.

We evaluated the utility of each new solvent to form and study single-molecule junctions using previously described custom-built STM-BJ instrumentation (see **SI** for additional details).[3,26,27] In the STM-BJ method, a gold STM tip is repeatedly pushed in and out of a gold substrate while applying a bias voltage (V) between the tip and substrate electrodes and using the measured current (I) to calculate conductance (G = I/V). Initial large area gold junctions thin with increasing tip-substrate displacement to produce single-atom point contacts, as indicated by step features in conductance-displacement traces with an average conductance of ~1 G_0 (= $2e^2/h$). In the presence of molecules that can bridge the electrodes, we form single-molecule junctions after breaking the point contact that result in additional step features at conductance values <1 G_0 (**Figure 1a**). We compile thousands of consecutively measured traces into conductance histograms without data selection, whereby the most probable conductance values and other characteristic features can be analyzed. For variable-temperature STM-BJ studies, we apply a custom-built resistive heating stage that controls the temperature of the substrate only (**SI, Figure S1**). At temperatures above RT, STM-BJ experiments are not easily conducted without solvent as the tip undergoes rapid thermal expansion and contraction when moved in and out of substrate contact. When both tip and substrate are in contact with solvent they reach thermal equilibrium in <15 min.

We initially targeted studies of **bipy** at RT as this is known to exhibit two conductance peaks associated with binding through different junction geometries.[20] The high conductance feature is attributed to the pyridyl group binding to gold at a small angle relative to the electrode surface, enhancing coupling between electrode states and the pyridyl π-system. The low conductance feature is associated with pyridyl binding perpendicular to the surface, through the N lone pair that is orthogonal to the π-system. In **Figure 1b**, we plot representative overlaid histograms for **bipy** measurements in TCB, DEHA and SQ. Data for the other solvents is provided in **SI, Figure S3**. Each histogram clearly shows the characteristic features of **bipy** junctions, and the absence of excessive background noise attributable to Faradaic and capacitive charging currents, confirming all solvents in **Table 1** are suitable for STM-BJ experiments.

These studies also reveal that the high and low conductance features of **bipy** junctions ($G_{\mathbf{bipy}}$) vary by a factor of ~2 when measured in different solvents (**Figure 1d** and **SI, Table S2**), and that $G_{\mathbf{bipy}}$ is typically lower in solvents comprising heteroatoms (Cl, Br, O). Following previous reports we suggest that these solvents, which are expected to bind more strongly to undercoordinated gold atoms, can effectively displace **bipy** from surface sites in the vicinity of the **bipy** junction.[10] This should reduce the surface dipole and decrease the local Fermi level

(E_F). For **bipy** junctions, whose conductance is dominated by transport through the lowest unoccupied molecular orbital (LUMO),[20,28] the increased energy difference between E_F and E_{LUMO} will result in a decrease in $G_{\mathbf{bipy}}$. This trend, as anticipated,[9] is opposite to that observed for 1,4-benzenediamine junctions where conductance is dominated by transport through the highest occupied molecular orbital.[10]

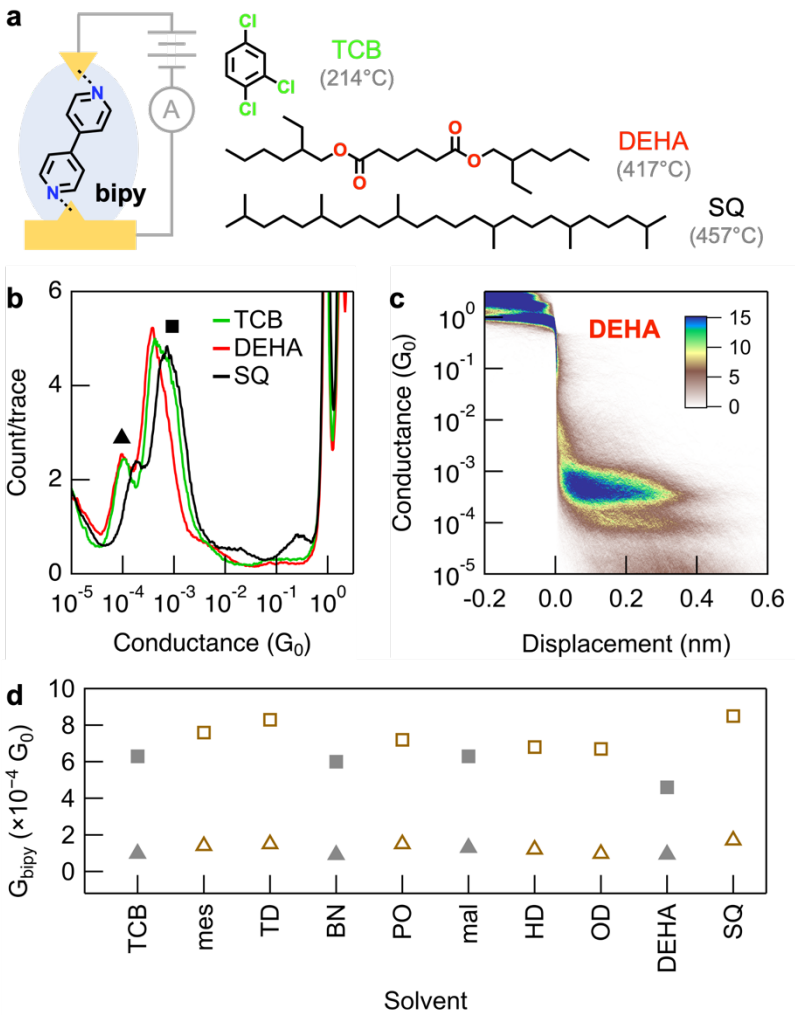

Figure 1. (a) *Left:* Schematic illustration of a 4,4'-bipyridine (**bipy**) single-molecule junction, formed through solution self-assembly using different solvents. *Right:* Molecular structures of commonly utilized 1,2,4-trichlorobenzene (TCB) and previously unreported bis(2-ethylhexyl)adipate (DEHA) and squalane (SQ) solvents (b.p. noted in parenthesis). **(b)** Overlaid 1D conductance histograms for **bipy** measured in TCB, DEHA, and SQ, each showing the double peak feature characteristic of these junctions (>8,000 traces, V_{bias} = 100 mV).[20] **(c)** The corresponding 2D conductance histogram for **bipy** measured in DEHA. Conductance data for **bipy** measured in the other solvents listed in **Table 1** are presented in the **SI, Figures S3-4**. **(d)** A plot of high (square) and low (triangle) conductance peak features in different solvents (see **Figure S5** and **Table S2** for details of peak fits). Junctions formed in solvents containing heteroatoms (solid) typically exhibit a lower conductance than solvents comprising only C and H atoms (hollow).

To benchmark DEHA and SQ as STM solvents for studies at elevated temperature, we first performed solution measurements of a thioether-terminated terphenyl wire (**P3SMe**, **Figure 2a**-inset). The tunneling conductance of junctions formed from such oligophenyl wires in TCB and PO solutions has been reported to increase with increasing temperature up to 73°C,

attributed to the thermally enhanced planarization of the oligophenyl backbone.[5] In **Figure 2a**, we present overlaid conductance histograms for **P3SMe** obtained in DEHA at RT (blue; 22-28°C) and 100°C (red) that corroborate these findings. However, we also observe a noticeable decrease in the intensity of both molecular junction and gold point contact peak features. Similar results are obtained for **P3SMe** measurements in SQ (**SI, Figure S6**), and for measurements of analogous (**PnSMe**) wires in DEHA (n = 2,4; **SI, Figure S7a,c**). Analysis of the corresponding 2D conductance-displacement histograms and junction step-lengths for **P3SMe** shows that this lower intensity junction peak results from a step feature that is 0.25 nm shorter (**Figure 2b-d**).

Given that the reduced intensity 1 G_0 peak at elevated temperature has been attributed to the increased mobility of gold surface atoms,[29–31] we hypothesized that shorter junction steps may be rationalized by an increased gold snapback distance under these conditions. This distance has been previously measured at room[20,22,32] and cryogenic[33,34] temperature(s), and results from the rapid restructuring of the gold interface to a lower energy configuration after rupturing the point contact. As junction step lengths correlate with the length of the molecular component after subtraction of the snapback distance, we expect the step length to decrease as the snapback distance increases. In **Figure 2f** we present overlaid snapback distance histograms from snapback measurements in DEHA at RT and 100°C (see **Figure 2e** and the **SI** for experimental details).[32] Peak fits confirm the average snapback distance at 100°C is 0.4 nm larger than at RT, providing a clear explanation for the shorter junction step lengths measured under these conditions.

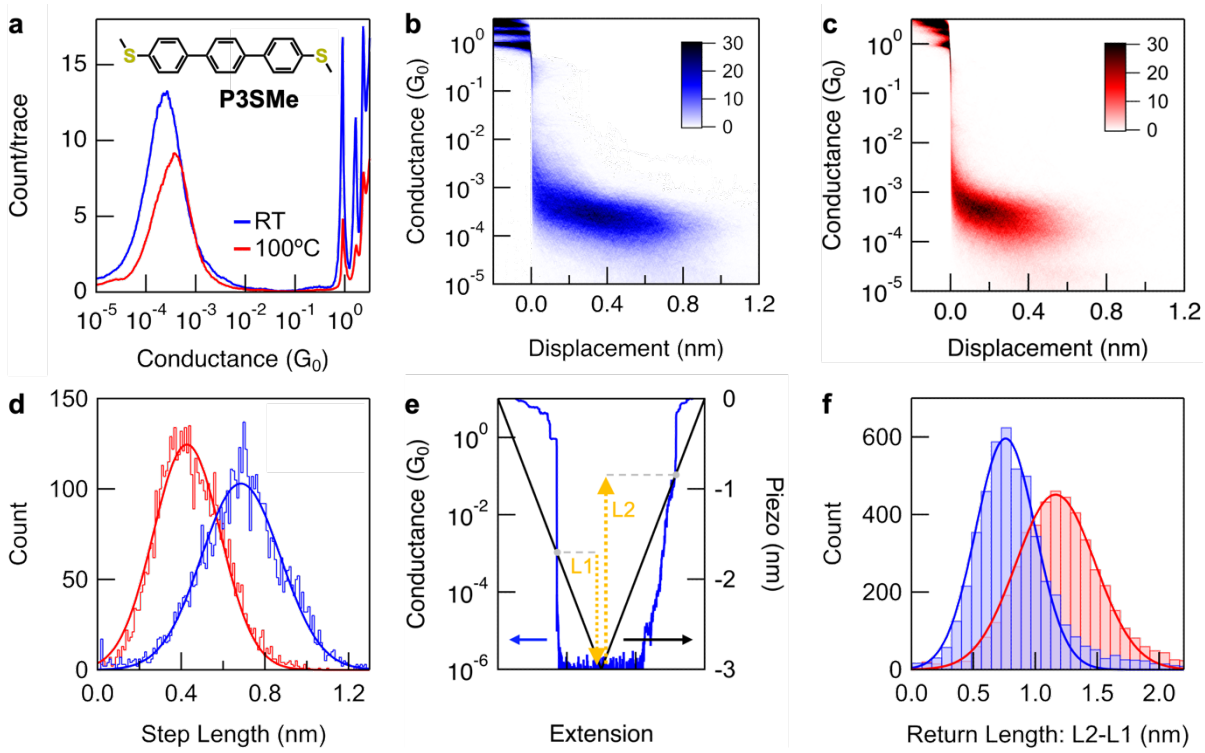

Figure 2. (a) Overlaid 1D conductance histograms (5,000 traces, V_{bias} = 100 mV) obtained for a 1 mM solution of **P3SMe** (structure inset) in DEHA at room temperature (RT, blue) or 100°C (red). At elevated temperatures, the molecular conductance peak shifts to higher conductance and decreases in intensity. (**b, c**) 2D conductance histograms corresponding to the histograms shown in (a). These show that the reduced intensity for molecular junction and gold point contact (~1 G_0) result from shorter step features. **(d)** Overlaid step length histograms with Gaussian fits (solid lines), obtained from the datasets used in (a-c). The average difference between junction step lengths is 0.25 nm. **(e)** In snapback measurements, a conductance-displacement trace (blue, left axis) is obtained with a piezo ramp (black, right axis) applied to move the tip out and back in to contact with the substrate in DEHA (no analyte molecules). L1 is the tip-substrate displacement between breaking the junction ($G < 0.9\ G_0$) and reversing the piezo direction, L2 is the displacement required to reform the junction ($G > 0.9\ G_0$). **(f)** Overlaid snapback distance histograms with solid line fits for L2-L1 (the gold snapback distance) at RT (blue, 0.76 nm) and 100°C (red, 1.16 nm). The difference in snapback between RT and 100°C is 0.40 nm, which is comparable to the average difference in junction step lengths (d).

To further demonstrate the utility of low vapor pressure solvents in STM-BJ studies, we apply them to probe the reactivity of phenylboronic acids exposed to gold surfaces at different temperatures. Building on reaction chemistry demonstrated using nanoparticle or supported gold catalysts,[35,36] Li *et al.* showed that thioether-terminated phenylboronic acids and esters are capable of undergoing transmetallation processes at the solution-electrode interface to form aryl-Au linked junctions during STM-BJ measurements.[21] These adsorbed

species can subsequently undergo surface-mediated $C(sp^2)$-$C(sp^2)$ homocoupling processes. Here, we determined to probe the temperature-dependance of these reactions *in situ* and explore whether the condensation of boronic acids to cyclotrimerized boroxine products could be driven through the elimination of H_2O at elevated temperatures (**Figure 4a**).[37]

In **Figure 3a** we plot overlaid conductance histograms for 4-methylthiophenylboronic acid (**P1B**) measured in DEHA at RT and 100°C. At RT our histograms are comparable to those previously reported from measurements of **P1B** in TCB,[21,27] showing a clear feature at 1×10^{-2} G_0 ("(i)") but only a broad peak at 6×10^{-4} G_0 ("(ii)"). Upon heating to 100°C, peak (ii) sharpens and increases in intensity, and we observe a new feature at 4×10^{-6} G_0 ("(iii)") that corresponds to a step that forms after breaking the step associated with peak (ii) (**Figure 3c**). Following earlier reports,[21] we attribute peak (i) to the Au-C bound transmetallation product and peak (ii) to junctions comprising the homo-coupled biphenyl species (**Figure 3b**). These assignments are further corroborated by the observation of comparable peak features in studies of 4-thioanisole-$AuPPh_3$ (comprising a pre-installed aryl-Au bond).[38] As indicated in **Figure 3b**, we attribute peak (iii) to π-stacked dimer junctions of **P2SMe**, noting that this feature is also observed in measurements of pure **P2SMe** in DEHA (**SI, Figure S7**). While measurements of **P1B** were performed with a tip-substrate bias of 750 mV to resolve peak (iii), the intensity of peaks (i) and (ii) similarly increase upon heating to 100°C at a bias of 100 mV (**SI, Figure S10**). This demonstrates that temperature is a particularly effective handle for driving such chemical reactions.

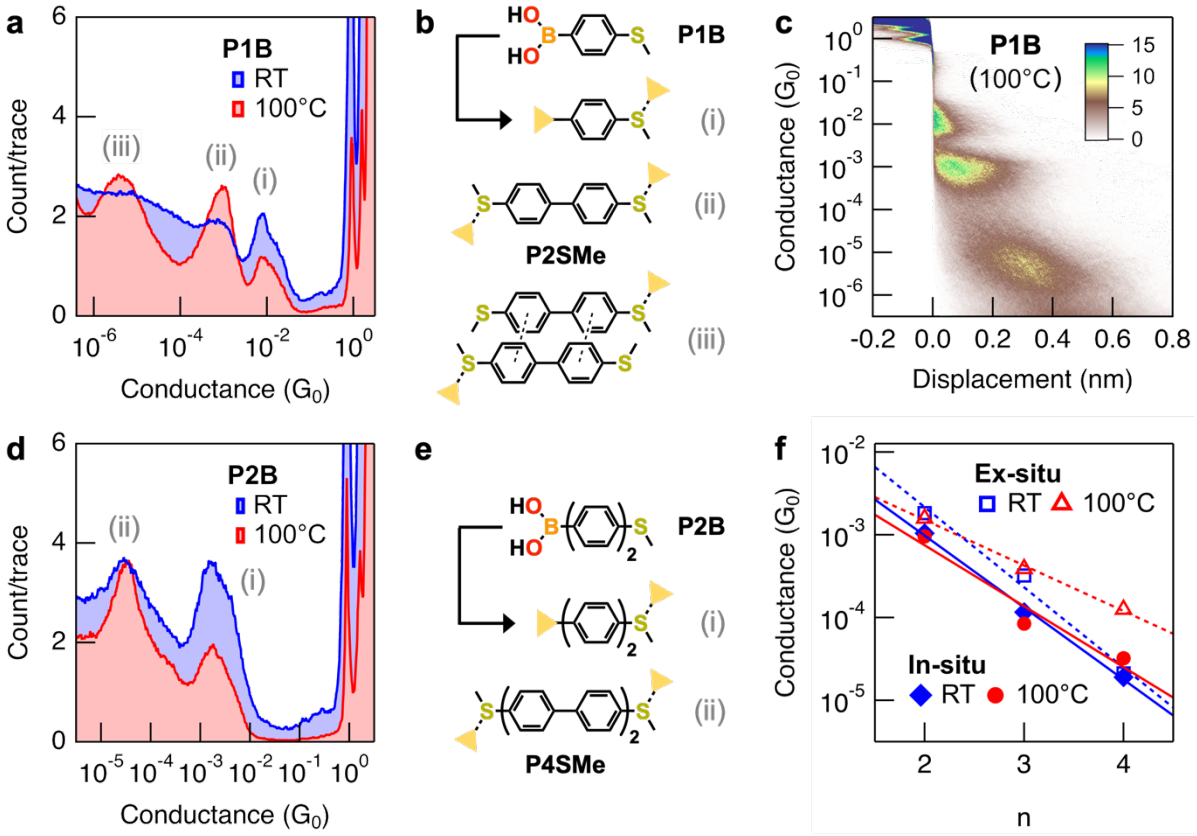

Figure 3. (a) Overlaid 1D conductance histograms (10,000 traces, V_{bias} = 750 mV) obtained for measurements of **P1B** solutions in DEHA measured at RT (blue) and 100°C (red). At elevated temperatures, a low intensity feature observed in RT measurements at 6×10^{-4} G_0 (ii) becomes more pronounced, and a new feature is observed at 4×10^{-6} G_0 (iii). **(b)** Proposed molecular junctions formed from **P1B**, following: (i) transmetallation of the phenyl group to gold; (ii) homocoupling of the transmetalated product to form **P2SMe**; (iii) π-stacking between two **P2SMe** molecules. **(c)** A 2D histogram for the measurement of **P1B** at 100°C, corresponding to the 1D histogram in (a). **(d)** Overlaid 1D histograms (5,000 traces, V_{bias} = 750 mV) for **P2B** measured in DEHA measured at RT (blue) and 100°C (red). **(e)** Proposed molecular junctions formed from **P2B**. **(f)** A plot of conductance versus n for measurements of **PnSMe** prepared *ex situ* (hollow/dotted) and *in situ* (solid) at RT (blue) and 100°C (red). *Ex situ* conductance values are an average of ≥2 measurements, *in situ* values are taken from a single measurement. Conductance and β values obtained from fits to $G = G_c e^{(-\beta n)}$, as well as additional conductance histograms, can be found in the **SI, Table S3** and **Figure S7-9**.

Comparable changes in peak features upon heating are observed for 4-(4-methylthiophenyl)phenylboronic acid (**P2B**), which we attribute to formation of the corresponding transmetallation product and **P4SMe** (**Figure 3d,e**). We also observe a feature that we attribute to **P3SMe** upon heating a mixture of **P1B** and **P2B** in DEHA (**SI, Figure S7e**). In **Figure 3f**, we overlay plots of the most probable conductance vs. n for measurements of **PnSMe** prepared *ex situ* and *in situ* at RT and 100°C. This analysis reveals that **PnSMe**

junctions prepared *in situ* exhibit a greatly reduced temperature-dependence compared to junctions formed from the *ex situ* synthesized species, suggesting that the presence of proximal chemisorbed Au-aryl species may hinder the enhanced planarization of phenyl rings at elevated temperatures. **Figure 3f** also shows that the conductance of **PnSMe** junctions prepared *in situ* is typically lower than that obtained for measurements of the wires synthesized *ex situ* using solutions comprising pure analyte material. We again attribute this small conductance change to the presence of chemisorbed Au-aryl species, which we hypothesize shifts the local E_F further from the dominant conducting orbital(s) of **PnSMe**.

Remarkably, conductance histograms of **P1B** obtained from measurements at 100°C, or even 110°C (**SI, Figure 11**), in air contain no peak features that may be assigned to the formation of the boroxine product **BOr** (**Figure 4a**), likely due to rapid transmetallation. To verify this observation, we synthesized **BOr** *ex situ* and subjected it to glovebox STM-BJ measurements in anhydrous DEHA at RT under an inert nitrogen atmosphere. The corresponding conductance histograms comprise a prominent new feature around 1×10^{-5} G_0 that we attribute to the formation of **BOr** junctions (**Figure 4b,c**). While a peak at ~1×10^{-2} G_0 is still apparent, the conspicuous absence of a feature attributable to **P2SMe** junctions at ~1×10^{-3} G_0 indicates the peak around 1×10^{-5} G_0 may not be attributed to the π-stacked **P2SMe** dimer geometry (**Figure 3a,b**). Remarkably, measurements of **P1B** under the same conditions yield comparable conductance histograms albeit with a more prominent feature at ~1×10^{-3} G_0. This indicates that, in contrast to measurements at ≥100°C, **BOr** readily forms *in situ* from solutions of **P1B** prepared in an anhydrous environment at RT which serves to shift the equilibrium in favor of the condensed species (**Figure 4a**). We note that the conductance of **BOr** junctions (1×10^{-5} G_0 in DEHA) is comparable to analogous components comprising 1,3-connected triazine or benzene central rings (2×10^{-5} G_0 and 6×10^{-6} G_0, respectively, in tetrahydrofuran/mes).[39] The lack of clear correlations between conductance and the difference in electronegativity of backbone heteroatoms in this family of molecules, observed for a variety of other compounds,[27,40,41] likely reflects a complex interplay of orbital (de)localization and destructive quantum interference in these cross-conjugated systems.[39,42,43]

These experiments appear to demonstrate that **P1B** can undergo the same interfacial chemistry under an inert nitrogen atmosphere as those observed during measurements in air, whereas control studies[21,44] and proposed mechanisms[21,45] suggest O_2 is key to activation of the boronic acid group. However, our glovebox STM-BJ studies are typically performed in the presence of O_2 at ppm concentrations,[27] so we cannot rule out the presence of adventitious oxygen adsorbed at the electrode-solution interface. DEHA also comprises ester groups which

could feasibly interact with gold in a similar manner to that proposed for O_2. To help evaluate this hypothesis, we present, in **Figure 4d**, conductance histograms obtained from glovebox STM-BJ measurements of **BOr** and **P1B** in anhydrous TD. These present analogous conductance features to those obtained from studies in DEHA, while peaks attributable to boronic acid activation do appear reduced in intensity. Unfortunately, it remains difficult to deconvolute other influences of the solvent environment on these interfacial reactions, such as the reduced solubility of analytes in TD compared to DEHA or the reduced polarity of TD which may destabilize charged intermediates.

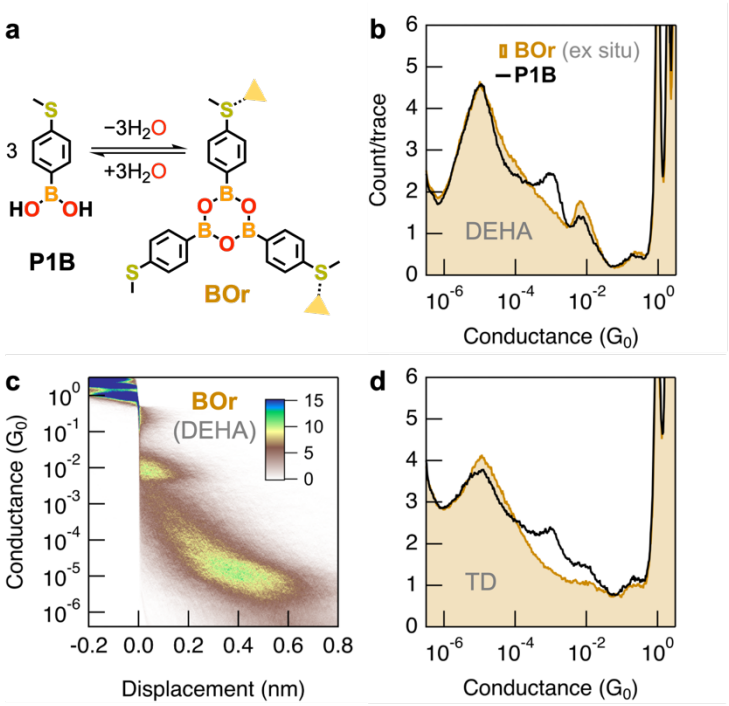

Figure 4. (a) A scheme showing the formation of **BOr** from **P1B** through a condensation reaction. This equilibrium can be driven to the right by the removal of water. **(b)** Overlaid 1D conductance histograms for **BOr** and **P1B** measured in anhydrous DEHA under an inert nitrogen atmosphere (10,000 traces, V_{bias} = 750 mV). **(c)** 2D histogram corresponding to the **BOr** measurement in panel (b). **(d)** Overlaid 1D conductance histograms for **BOr** and **P1B** measured in anhydrous TD under an inert nitrogen atmosphere (10,000 traces, V_{bias} = 750 mV). These measurements reveal a new conductance feature around 1×10^{-5} G_0 that is attributable to the formation of **BOr** junctions in the absence of water at RT.

In summary, we have shown that low toxicity, ultrahigh b.p. solvents such as DEHA and SQ can be used to routinely perform STM-BJ measurements in solution at 100°C. We find, in proof-of-concept studies using common analytes such as **bipy** and **PnSMe**, these solvents are readily applied to reproduce and extend previously reported solvent- and temperature-

dependent conductance trends. Critically, we also show that the increased mobility of gold atoms at 100°C results in an increased snapback distance that significantly reduces molecular junction step lengths. In demonstrating that temperature can be applied in STM-BJ studies to drive and study chemical reactions, we show that the oligophenyl products formed *in situ* from the coupling of aryl boronic acids exhibit distinct conductance properties to the isolated species synthesized *ex situ*. We anticipate that the new capabilities provided by these or other ultrahigh b.p. solvents will strongly motivate additional investigations that target single-molecule devices or interfacial chemistry controlled through temperature modulation or extended molecule-electrode contact. As demonstrated here, such studies can provide new insights into junction characteristics and surface-based reaction mechanisms critical to the effective exploitation of these nanoscale functional assemblies and interfacial processes.

ASSOCIATED CONTENT

Electronic Supplementary Information (ESI) available: Additional experimental details, solvent evaporation studies, synthetic methods, and conductance data.

AUTHOR INFORMATION

Corresponding Author

Michael S. Inkpen – Email: inkpen@usc.edu

Notes

The authors declare no competing financial interest.

ACKNOWLEDGEMENTS

This work was primarily supported by funding from the University of Southern California (USC) and the National Science Foundation (NSF CAREER Award to M.S.I., CHE-2239614). K.N. and S.S. thank the NSF CAREER program, Agilent Technologies, and Steve and Cathy Gagliardi for their support of the USC-Cerritos Summer Internship in Sustainability program. Instrumentation in the USC Chemistry Instrument Facility was acquired with support from the USC Research and Innovation Instrumentation Award Program. Additionally, funds provided by the NSF (DBI-0821671, CHE-0840366) and National Institute of Health (S10 RR25432)

supported the acquisition of the NMR spectrometers used in our work. We are grateful to Nils Rotthowe for useful discussions.

REFERENCES

(1) Mali, K. S.; Adisoejoso, J.; Ghijsens, E.; De Cat, I.; De Feyter, S. Exploring the Complexity of Supramolecular Interactions for Patterning at the Liquid–Solid Interface. *Acc. Chem. Res.* **2012**, *45* (8), 1309–1320. https://doi.org/10.1021/ar200342u.

(2) Mamdouh, W.; Uji-i, H.; Ladislaw, J. S.; Dulcey, A. E.; Percec, V.; De Schryver, F. C.; De Feyter, S. Solvent Controlled Self-Assembly at the Liquid-Solid Interface Revealed by STM. *J. Am. Chem. Soc.* **2006**, *128* (1), 317–325. https://doi.org/10.1021/ja056175w.

(3) Venkataraman, L.; Klare, J. E.; Tam, I. W.; Nuckolls, C.; Hybertsen, M. S.; Steigerwald, M. L. Single-Molecule Circuits with Well-Defined Molecular Conductance. *Nano Lett* **2006**, *6* (3), 458–462. https://doi.org/10.1021/nl052373+.

(4) Millar, D.; Venkataraman, L.; Doerrer, L. H. Efficacy of Au−Au Contacts for Scanning Tunneling Microscopy Molecular Conductance Measurements. *J Phys Chem C* **2007**, *111* (47), 17635–17639. https://doi.org/10.1021/jp0756101.

(5) Lee, W.; Louie, S.; Evans, A. M.; Orchanian, N. M.; Stone, I. B.; Zhang, B.; Wei, Y.; Roy, X.; Nuckolls, C.; Venkataraman, L. Increased Molecular Conductance in Oligo[n]Phenylene Wires by Thermally Enhanced Dihedral Planarization. *Nano Lett* **2022**, *22* (12), 4919–4924. https://doi.org/10.1021/acs.nanolett.2c01549.

(6) Nagahara, L. A.; Thundat, T.; Lindsay, S. M. Preparation and Characterization of STM Tips for Electrochemical Studies. *Rev. Sci. Instrum.* **1989**, *60* (10), 3128–3130. https://doi.org/10.1063/1.1140590.

(7) Greenwald, J. E.; Cameron, J.; Findlay, N. J.; Fu, T.; Gunasekaran, S.; Skabara, P. J.; Venkataraman, L. Highly Nonlinear Transport across Single-Molecule Junctions via Destructive Quantum Interference. *Nat. Nanotechnol.* **2021**, *16* (3), 313–317. https://doi.org/10.1038/s41565-020-00807-x.

(8) Nakashima, S.; Takahashi, Y.; Kiguchi, M. Effect of the Environment on the Electrical Conductance of the Single Benzene-1,4-Diamine Molecule Junction. *Beilstein J. Nanotechnol.* **2011**, *2*, 755–759. https://doi.org/10.3762/bjnano.2.83.

(9) Kotiuga, M.; Darancet, P.; Arroyo, C. R.; Venkataraman, L.; Neaton, J. B. Adsorption-Induced Solvent-Based Electrostatic Gating of Charge Transport through Molecular Junctions. *Nano Lett.* **2015**, *15* (7), 4498–4503. https://doi.org/10.1021/acs.nanolett.5b00990.

(10) Fatemi, V.; Kamenetska, M.; Neaton, J. B.; Venkataraman, L. Environmental Control of Single-Molecule Junction Transport. *Nano Lett.* **2011**, *11* (5), 1988–1992. https://doi.org/10.1021/nl200324e.

(11) Dalmieda, J.; Shi, W.; Li, L.; Venkataraman, L. Solvent-Mediated Modulation of the Au–S Bond in Dithiol Molecular Junctions. *Nano Lett.* **2024**, *24* (2), 703–707. https://doi.org/10.1021/acs.nanolett.3c04058.

(12) Choi, B.; Capozzi, B.; Ahn, S.; Turkiewicz, A.; Lovat, G.; Nuckolls, C.; Steigerwald, M. L.; Venkataraman, L.; Roy, X. Solvent-Dependent Conductance Decay Constants in Single Cluster Junctions. *Chem. Sci.* **2016**, *7* (4), 1384–1389. https://doi.org/10.1039/C5SC02595H.

(13) Zhang, W.; Gan, S.; Vezzoli, A.; Davidson, R. J.; Milan, D. C.; Luzyanin, K. V.; Higgins, S. J.; Nichols, R. J.; Beeby, A.; Low, P. J.; Li, B.; Niu, L. Single-Molecule

Conductance of Viologen–Cucurbit[8]Uril Host–Guest Complexes. *ACS Nano* **2016**, *10* (5), 5212–5220. https://doi.org/10.1021/acsnano.6b00786.
(14) Migliore, A.; Nitzan, A. Nonlinear Charge Transport in Redox Molecular Junctions: A Marcus Perspective. *ACS Nano* **2011**, *5* (8), 6669–6685. https://doi.org/10.1021/nn202206e.
(15) Rashid, U.; Bro-Jørgensen, W.; Harilal, K.; Sreelakshmi, P.; Mondal, R. R.; Chittari Pisharam, V.; Parida, K. N.; Geetharani, K.; Hamill, J. M.; Kaliginedi, V. Chemistry of the Au–Thiol Interface through the Lens of Single-Molecule Flicker Noise Measurements. *J. Am. Chem. Soc.* **2024**, *146* (13), 9063–9073. https://doi.org/10.1021/jacs.3c14079.
(16) Zang, Y.; Zou, Q.; Fu, T.; Ng, F.; Fowler, B.; Yang, J.; Li, H.; Steigerwald, M. L.; Nuckolls, C.; Venkataraman, L. Directing Isomerization Reactions of Cumulenes with Electric Fields. *Nat. Commun.* **2019**, *10* (1), 4482. https://doi.org/10.1038/s41467-019-12487-w.
(17) Roldan, D.; Kaliginedi, V.; Cobo, S.; Kolivoska, V.; Bucher, C.; Hong, W.; Royal, G.; Wandlowski, T. Charge Transport in Photoswitchable Dimethyldihydropyrene-Type Single-Molecule Junctions. *J. Am. Chem. Soc.* **2013**, *135* (16), 5974–5977. https://doi.org/10.1021/ja401484j.
(18) Ho Choi, S.; Kim, B.; Frisbie, C. D. Electrical Resistance of Long Conjugated Molecular Wires. *Science* **2008**, *320* (5882), 1482–1486. https://doi.org/10.1126/science.1156538.
(19) Lörtscher, E. Reaction: Technological Aspects of Molecular Electronics. *Chem* **2017**, *3* (3), 376–377. https://doi.org/10.1016/j.chempr.2017.08.016.
(20) Quek, S. Y.; Kamenetska, M.; Steigerwald, M. L.; Choi, H. J.; Louie, S. G.; Hybertsen, M. S.; Neaton, J. B.; Venkataraman, L. Mechanically Controlled Binary Conductance Switching of a Single-Molecule Junction. *Nat. Nanotechnol.* **2009**, *4* (4), 230–234. https://doi.org/10.1038/nnano.2009.10.
(21) Li, Y.; Zhao, C.; Wang, R.; Tang, A.; Hong, W.; Qu, D.; Tian, H.; Li, H. In Situ Monitoring of Transmetallation in Electric Potential-Promoted Oxidative Coupling in a Single-Molecule Junction. *CCS Chem.* **2022**, *5*, 191–199. https://doi.org/10.31635/ccschem.022.202101757.
(22) Hong, W.; Manrique, D. Z.; Moreno-García, P.; Gulcur, M.; Mishchenko, A.; Lambert, C. J.; Bryce, M. R.; Wandlowski, T. Single Molecular Conductance of Tolanes: Experimental and Theoretical Study on the Junction Evolution Dependent on the Anchoring Group. *J Am Chem Soc* **2011**, *134* (4), 2292–2304. https://doi.org/10.1021/ja209844r.
(23) Camarasa-Gomez, M.; Hernangomez-Perez, D.; Inkpen, M.; Lovat, G.; Fung, E.-D.; Roy, X.; Venkataraman, L.; Evers, F. Mechanically-Tunable Quantum Interference in Ferrocene-Based Single-Molecule Junctions. *Nano Lett.* **2020**, *20* (9), 6381–6386.
(24) Jung, J.; Cho, Y.; Lee, Y.; Choi, K. Uses and Occurrences of Five Major Alternative Plasticizers, and Their Exposure and Related Endocrine Outcomes in Humans: A Systematic Review. *Crit. Rev. Environ. Sci. Technol.* **2024**, 1–30. https://doi.org/10.1080/10643389.2024.2301922.
(25) Final Report on the Safety Assessment of Squalane and Squalene. *J. Am. Coll. Toxicol.* **1990**, *1* (2), 37–56. https://doi.org/10.3109/10915818209013146.
(26) Inkpen, M. S.; Liu, Z.; Li, H.; Campos, L. M.; Neaton, J. B.; Venkataraman, L. Non-Chemisorbed Gold–Sulfur Binding Prevails in Self-Assembled Monolayers. *Nat. Chem.* **2019**, *11*, 351–358.

(27) Miao, Z.; Quainoo, T.; Czyszczon-Burton, T. M.; Rotthowe, N.; Parr, J. M.; Liu, Z.; Inkpen, M. S. Charge Transport across Dynamic Covalent Chemical Bridges. *Nano Lett* **2022**, *22* (20), 8331–8338. https://doi.org/10.1021/acs.nanolett.2c03288.
(28) Capozzi, B.; Chen, Q.; Darancet, P.; Kotiuga, M.; Buzzeo, M.; Neaton, J. B.; Nuckolls, C.; Venkataraman, L. Tunable Charge Transport in Single-Molecule Junctions via Electrolytic Gating. *Nano Lett* **2014**, *14* (3), 1400–1404. https://doi.org/10.1021/nl404459q.
(29) Zang, Y.; Fung, E.; Fu, T.; Ray, S.; Garner, M. H.; Borges, A.; Steigerwald, M. L.; Patil, S.; Solomon, G.; Venkataraman, L. Voltage-Induced Single-Molecule Junction Planarization. *Nano Lett* **2021**, *21* (1), 673–679. https://doi.org/10.1021/acs.nanolett.0c04260.
(30) Huang, Z.; Chen, F.; D'agosta, R.; Bennett, P. A.; Di Ventra, M.; Tao, N. Local Ionic and Electron Heating in Single-Molecule Junctions. *Nat. Nanotechnol.* **2007**, *2* (11), 698–703. https://doi.org/10.1038/nnano.2007.345.
(31) Tsutsui, M.; Taniguchi, M.; Kawai, T. Local Heating in Metal−Molecule−Metal Junctions. *Nano Lett.* **2008**, *8* (10), 3293–3297. https://doi.org/10.1021/nl801669e.
(32) Kim, T.; Vázquez, H.; Hybertsen, M. S.; Venkataraman, L. Conductance of Molecular Junctions Formed with Silver Electrodes. *Nano Lett.* **2013**, *13* (7), 3358–3364. https://doi.org/10.1021/nl401654s.
(33) Kamenetska, M.; Widawsky, J. R.; Dell'Angela, M.; Frei, M.; Venkataraman, L. Temperature Dependent Tunneling Conductance of Single Molecule Junctions. *J. Chem. Phys.* **2017**, *146* (9). https://doi.org/10.1063/1.4973318.
(34) Yanson, A. I.; Rubio Bollinger, G.; Van Den Brom, H. E.; Agraït, N.; Van Ruitenbeek, J. M. Formation and Manipulation of a Metallic Wire of Single Gold Atoms. *Nature* **1998**, *395* (6704), 783–785. https://doi.org/10.1038/27405.
(35) Carrettin, S.; Guzman, J.; Corma, A. Supported Gold Catalyzes the Homocoupling of Phenylboronic Acid with High Conversion and Selectivity. *Angew. Chem. Int. Ed.* **2005**, *44* (15), 2242–2245. https://doi.org/10.1002/anie.200462560.
(36) Tsunoyama, H.; Sakurai, H.; Ichikuni, N.; Negishi, Y.; Tsukuda, T. Colloidal Gold Nanoparticles as Catalyst for Carbon−Carbon Bond Formation: Application to Aerobic Homocoupling of Phenylboronic Acid in Water. *Langmuir* **2004**, *20* (26), 11293–11296. https://doi.org/10.1021/la0478189.
(37) Defrancesco, H.; Dudley, J.; Coca, A. Boron Chemistry: An Overview. *ACS Symp. Ser.* **2016**, *1236*, 1–25. https://doi.org/10.1021/bk-2016-1236.ch001.
(38) Starr, R. L.; Fu, T.; Doud, E. A.; Stone, I.; Roy, X.; Venkataraman, L. Gold–Carbon Contacts from Oxidative Addition of Aryl Iodides. *J. Am. Chem. Soc.* **2020**, *142* (15), 7128–7133. https://doi.org/10.1021/jacs.0c01466.
(39) Qu, F.-Y.; Zhao, Z.-H.; Ren, X.-R.; Zhang, S.-F.; Wang, L.; Wang, D. Multiple Heteroatom Substitution Effect on Destructive Quantum Interference in Tripodal Single-Molecule Junctions. *Phys. Chem. Chem. Phys.* **2022**, *24* (43), 26795–26801. https://doi.org/10.1039/D2CP03902H.
(40) Brisendine, J. M.; Refaely-Abramson, S.; Liu, Z.-F.; Cui, J.; Ng, F.; Neaton, J. B.; Koder, R. L.; Venkataraman, L. Probing Charge Transport through Peptide Bonds. *J. Phys. Chem. Lett.* **2018**, *9* (4), 763–767. https://doi.org/10.1021/acs.jpclett.8b00176.
(41) Li, H.; Garner, M. H.; Su, T. A.; Jensen, A.; Inkpen, M. S.; Steigerwald, M. L.; Venkataraman, L.; Solomon, G. C.; Nuckolls, C. Extreme Conductance Suppression in Molecular Siloxanes. *J. Am. Chem. Soc.* **2017**, *139* (30), 10212–10215. https://doi.org/10.1021/jacs.7b05599.

(42) Mayor, M.; Weber, H. B.; Reichert, J.; Elbing, M.; von Hanisch, C.; Beckmann, D.; Fisher, M. Electric Current through a Molecular Rod - Relevance of the Position of the Anchor Groups. *Angew Chem Int Ed Engl* **2003**, *42*, 5834–5838.
(43) Solomon, G. C.; Herrmann, C.; Hansen, T.; Mujica, V.; Ratner, M. A. Exploring Local Currents in Molecular Junctions. *Nat. Chem.* **2010**, *2*, 223–228.
(44) Wang, L.; Zhang, W.; Sheng Su, D.; Meng, X.; Xiao, F.-S. Supported Au Nanoparticles as Efficient Catalysts for Aerobic Homocoupling of Phenylboronic Acid. *Chem. Commun.* **2012**, *48* (44), 5476. https://doi.org/10.1039/c2cc31115a.
(45) Karanjit, S.; Ehara, M.; Sakurai, H. Mechanism of the Aerobic Homocoupling of Phenylboronic Acid on Au_{20}^{-}: A DFT Study. *Chem. – Asian J.* **2015**, *10* (11), 2397–2403. https://doi.org/10.1002/asia.201500535.